

Probing criticality with deep learning in relativistic heavy-ion collisions

Yi-Ge Huang,¹ Long-Gang Pang,^{1,*} Xiaofeng Luo,^{1,†} and Xin-Nian Wang^{1,2,‡}

¹*Key Laboratory of Quark and Lepton Physics (MOE) & Institute of Particle Physics,
Central China Normal University, Wuhan 430079, China*

²*Nuclear Science Division, Lawrence Berkeley National Laboratory, Berkeley, CA 94720, USA*

Systems with different interactions could develop the same critical behaviour due to the underlying symmetry and universality. Using this principle of universality, we can embed critical correlations modeled on the 3D Ising model into the simulated data of heavy-ion collisions, hiding weak signals of a few inter-particle correlations within a large particle cloud. Employing a point cloud network with dynamical edge convolution, we are able to identify events with critical fluctuations through supervised learning, and pick out a large fraction of signal particles used for decision-making in each single event.

I. INTRODUCTION

Quantum Chromodynamics (QCD) is the fundamental theory of the strong interaction. Exploring the phase structure of QCD matter is one of the main goals of heavy-ion collision experiment [1–3]. The most recent lattice QCD studies [4–6] predict an equation of state (EoS) with a rapid chiral cross over at temperature $T_c \approx 132$ MeV and nearly zero baryon chemical potential. At finite temperature and baryon density, QCD based models [7–10] predict that there is a possible QCD critical point (CP), which is the end point of the rapid cross over and the beginning of a first-order phase transition boundary between normal nuclear matter and quark-gluon plasma (QGP). Searching for the CP is the most important aspect of the experimental efforts to explore the QCD phase structure at the beam energy scan (BES) energies at the Relativistic Heavy-ion Collider (RHIC) [1–3].

Many theoretical and experimental devoted to locate the CP [11, 12]. One avenue is to classify the smooth crossover and first order phase transition using the information from the final state particle spectra and collective flow [13–25]. This method looks for the consequences of the softening of the equation of state since the pressure gradients are much smaller in a medium with a first order phase transition than a crossover phase transition, which leads to slower fluid acceleration and smaller transverse momenta of final state particles. Another avenue is to search for the enhanced fluctuations when the system goes through the critical point. These includes, for example, fluctuations of conserved charges [26–33], hydrodynamic fluctuations [34–36], fluctuations caused by spinodal instabilities [37–47] and enhanced light nuclei yield ratio due to baryon density fluctuations [48–51].

Many critical phenomena in systems with different interactions can develop the same critical behaviour with a universality that is dictated by the symmetry of the

systems and can be described by same critical exponents [52]. Lee and Yang proved that the Ising model in a magnetic field and a lattice gas are mathematically equivalent [53]. Employing this universality, one can therefore map the QCD equation of state to that given by a 3-dimensional Ising model with the same universality class [11, 53–57] to study the QCD phase diagram. The divergence of the correlation length near the critical point will lead to the critical opalescence and scaling invariant, which means that the systems are self-similar when the resolution changes. One thus expects that particles from the freeze-out hyper-surface close to the critical point have multi-particle fractal structure in the momentum space [58–62]. Experimentally, intermittency analysis has been proposed to probe the self-similarity and density fluctuations in heavy-ion collisions. Though a non-trivial intermittency phenomenon is observed recently by the NA61/SHINE experiment at CERN SPS [63–65] in Ar+Sc collisions at 150 AGeV, the magnitude of background fluctuations is big and the power law scaling is not fully established. No intermittency signal is observed in C+C, Pb+Pb and Be+Be collisions with similar collision energies. Critical Monte Carlo simulations suggest a maximum critical proton fraction smaller than 0.3% in Be+Be collision, indicating that traditional intermittency analysis may fail in looking for the weak signal of self-similarity, if the fraction of critical particles is small compared with uncorrelated background. It is interesting to explore whether the state-of-the-art deep learning can help to identify the weak intermittency signal from each event of heavy ion collisions.

Recently deep learning has been used to study the QCD equation of states by classifying phase transition types, using convolution neural network [66–69] and point cloud network [70, 71]. In heavy ion collisions at low energies, auto-encoder with a single latent variable is also used to study the order parameter of the nuclear liquid-gas phase transition [72]. In these studies, deep learning is powerful in mapping momentum or charge distributions of particles to the type of QCD phase transitions. In this study, we will train a dynamical edge convolution network plus a point cloud network to identify weak intermittency signals of critical fluctuations,

* lgpang@ccnu.edu.cn

† xfluo@ccnu.edu.cn

‡ xnwang@lbl.gov

from exotic uncorrelated background particles. Employing Critical Monte Carlo (CMC) [61, 62], we encode the self-similarity in the inter-particle distances in momentum space. Further, we assume that only a small fraction of particles have intermittency which does not change the single particle distribution.

This paper is organized as follows. In Sec. II, we present the JAM transport model which is used to generate data on multiple particle production in heavy ion collisions. The CMC is used to generate intermittency signals of critical fluctuations and the deep neural network is used for both classification and tagging. In Sec. III, the prediction accuracy is compared for point cloud network and dynamical edge convolution neural network. We also show the performance of signal-particle tagging. In Sec. IV, we discuss and summarize the findings and the implications of the present work.

II. METHOD

Probing critical fluctuations in high energy heavy ion collisions is a typical inverse problem. The information of a critical point should be transmitted through the dynamical evolution of the dense medium in heavy ion collisions and get encoded in the hadron cloud that are detected in an experiment. In the forward process, relativistic hydrodynamics as well as quantum molecular dynamics are widely used to generate single particle distribution and multi-hadron correlations, which are normally used to constrain the model parameters against the experimental data. In the present study, we use the JAM[73, 74] model that is well tested for low and intermediate energy heavy ion collisions to generate data without critical fluctuations. Critical fluctuations from a Critical Monte-Carlo (CMC) model [61, 62] are encoded in equal amount of JAM events.

In the inverse process, a point cloud network and a dynamical edge convolution network are trained to identify critical fluctuations encoded in the intermittency of a small fraction of particles (5% or 10%), from large amount of uncorrelated background particles.

A. JAM model for heavy ion collisions

JAM is one of the hadronic transport models widely used to simulate low beam energy heavy-ion collisions [73–82]. It simulates the complicated process from initial stage nuclear collisions to multiple particle production and final state hadronic interactions. Independent binary collisions among hadrons including produced ones are modeled using the vacuum hadron-hadron scattering cross section. Different from traditional cascade models, particles in JAM do not move along straight lines at the time intervals of collisions. They move in a nuclear mean field based on the simplified version of the relativistic quantum molecular dynamics. In the latest version, it

is also possible to control the pressure of the system by modifying two-body interaction types, to simulate a first order phase transition as well as a smooth crossover in an equation of state (EoS).

In the present study, we use JAM to generate 2.3×10^5 events of Au+Au central collisions with impact parameters $b < 3$ fm, at center of mass energy per pair of nucleons $\sqrt{s_{NN}} = 27$ GeV. Each event consists of hundreds of charged particles whose species include pion, kaon and proton. The transverse momentum p_x and p_y in GeV/c. are considered as 2 features of each particle. In this case, each event stores one particle cloud in 2-dimensional momentum space. 2×10^5 events are used to form the training set, while 1×10^4 are validation set and 2×10^4 are test set. For each JAM event, a corresponding event is created that encodes the critical fluctuation signal from the CP. As a result, 4.6×10^5 events in total are used in our study. It is computationally expensive to generate many new JAM events to encode critical fluctuations. To avoid data pollution, event with critical fluctuations and its corresponding JAM event are always put in the same data set. In this case, if one JAM event is in the training data, the event with critical fluctuations associated with that JAM event is also put in the training data. We will refer to these events with critical fluctuations as critical events and these particles encoded with the critical fluctuations as critical particles.

B. Critical Monte-Carlo model

Critical Monte-Carlo (CMC) model [61, 62, 83] can simulate events which involve critical fluctuations in the baryon density, by generating baryons whose momenta are correlated according to a power law function,

$$f(p) = \frac{\nu p_{\min}^\nu}{1 - (p_{\min}/p_{\max})^\nu} p^{-1-\nu} = A p^{-\alpha} \quad (1)$$

where p is the distance of two critical particles in momentum space, $\nu = 1/6$ is an index related to the universality class of 3D Ising model, p_{\min} and p_{\max} are the minimum and maximum distances between two adjacent particles. In the second equation, $\alpha = 1 + \nu$ and A is the coefficient independent of p .

Starting with an arbitrary particle in a JAM event, the Levy flight random walk algorithm proposes the next step with strides respecting the distribution $f(p) = A p^{-\alpha}$. In this way, a sequence of critical particles are generated whose adjacent differences Δp_T obey the power law distribution. The self-similarity or intermittency is thus encoded in these critical particles, which can be proved to be closely related to the observed large baryon density fluctuations associated with the critical point. To minimize the effect on single particle distribution, we set $p_{\min} = 1 \times 10^{-7}$ GeV/c and $p_{\max} = 1$ GeV/c.

The scaled factorial moments (SFM), which measure the power law of intermittency behaviors in multiple par-

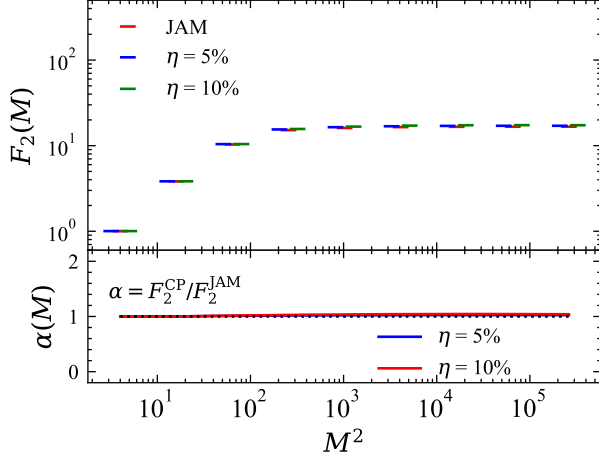


FIG. 1. The second order scaled factorial moments analysis (SFM) for uncorrelated JAM events and events with critical fluctuations. The upper-panel shows the absolute values of SFM for JAM events and events with 5% and 10% critical particles. To avoid the overlap of markers, results of critical events are slightly shifted for a clearer visualization. The lower-panel shows the ratios between critical and normal JAM events. No significant differences are observed for the absolute SFM values and their ratios.

ticle production in heavy ion collision, are defined as follows,

$$F_q(M) = \frac{\langle \frac{1}{M^D} \sum_{i=1}^{M^D} n_i(n_i-1) \cdots (n_i-q+1) \rangle}{\langle \frac{1}{M^D} \sum_{i=1}^{M^D} n_i \rangle^q} \quad (2)$$

where M is the number of grids in momentum space with equal size, D is the dimension, i is the number of particles in the i 'th momentum-grid, and q is the order of the SFM method. In the present study, the second order SFM ($q = 2$) in two dimensional space ($D = 2$) are studied for $M = 2, 4, 8, 16, 32, 64, 128, 256$ and 512 .

As shown in Figure. 1, the intermittency analysis using the SFM method [62–65] can not differentiate CP events with 5% and 10% critical particles that carry critical fluctuations from uncorrelated JAM events.

C. Dynamical edge convolution neural network

A graph-based dynamical edge convolution neural network is trained for our multi-task learning. The input to the neural network are the particle cloud of each event, which consists of a list of particles with their information on (p_x, p_y) . The output of the neural network corresponds to two tasks. The first task is the binary classification which requires true labels of each single event for supervised learning, with CP indicating events with critical fluctuations and JAM indicating events without. The second task is the particle tagging which requires true labels of each single particle, with 0 or 1 to indicate

whether the particle is generated using Critical Monte Carlo model.

Shown in Figure. 2 is the architecture of our neural network. There are two kNN plus dynamical edge convolution blocks connecting to the input layer. In the first block, kNN is used to find the k -nearest neighbors of each particle in (p_x, p_y) space. A fully connected network is used to learn edge features $\phi(\vec{p}_i, \vec{p}_j)$ between the i 'th particle and its j 'th neighbor. This module is shared by all its neighbors of particle i to produced edge features and that explains the name "edge convolution". The information of particle i together with its edge features are feed to the second block. Edge convolution layer would not only make use of the features of input neuron itself, but also take the relevance between the clustered units near that neuron into consideration, thus it can effectively capture the correlation information between particles.

The second kNN find the k -nearest neighbors of each particle in feature space. It is thus possible to correlate particles that are far away in momentum space. The neighbors of each particle change dynamically when the distances are computed in feature space, that is why the method is called "dynamical edge convolution".

The features of each particle together with its "local" information are flattened and feed to a fully connected neural network to get a high dimensional latent variable for each particle. The latent variable provides a high dimensional representation of each particle. The above neural network is also shared by all particles and is called 1D convolution neural network (CNN). Finally, the latent variables of each particle are used for two different tasks. The module of "Classification" task is shown in the lower right corner. A global max pooling gets the maximum values of each feature among all particles. This symmetric permutation operation learns the global feature of each particle cloud and is used to determine whether it is a CP or JAM event. The module of "Tagging" task is shown on the right of Figure. 2. A 1D CNN with one output neuron is used to tag each particle in the particle cloud. This module provides interpretation on whether the correlated particles are used to identify events with critical fluctuations. We have labeled correlated critical particles as "signal" and uncorrelated JAM particles as "noise". Binary cross entropy is used to compute the differences between the tagging output and the true labels of each particle. The loss values of tagging module is added to the total loss with a weighting factor 10^{-3} such that the network focus more on "classification" task.

For comparison, we also train a point-cloud network without the kNN and dynamical edge convolution blocks shown in Figure. 2. The (p_x, p_y) of each particle is directly feed to 1D CNN with 256, 128 and 64 channels respectively for classification. Global average pooling layer is used in this simple point-cloud network as it performs better here. Without kNN and dynamical edge convolution, the network can not capture much local information for intermittency identification.

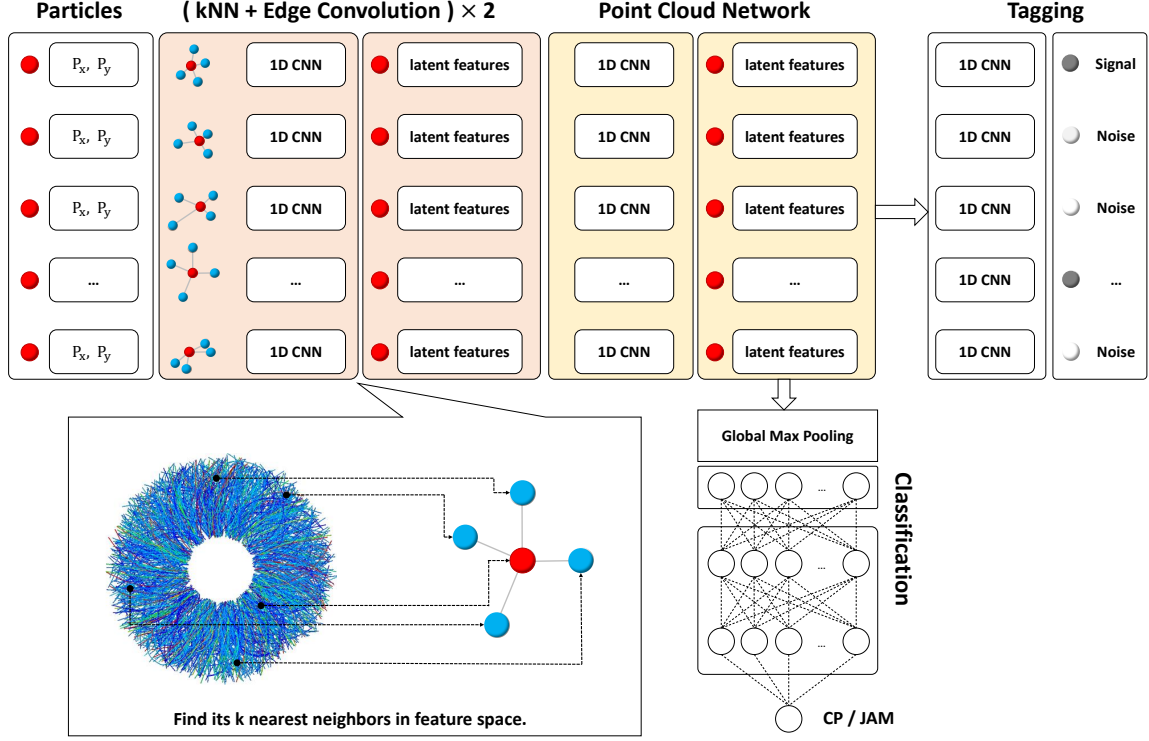


FIG. 2. Dynamical edge convolution neural network with point cloud module for both classification and tagging. The edge convolution block looks for k nearest neighbors of each particle to obtain a latent representation of that very particle, with short or long range correlations encoded deeply in. The representation of each particle are used in two tasks. One is the classification task to identify critical fluctuations from uncorrelated background events. The other is the tagging task to label correlated particles used for decision making.

III. RESULTS AND DISCUSSION

A. Classification accuracy

Shown in the Figure. 3 are the training (solid lines) and validation (dashed lines) accuracy as a function of training epochs. Both training and validation accuracy increase as the model is trained longer with more epochs. The validation accuracy reaches a maximum of 98.0%, which means that deep learning is able to classify each single event with high accuracy, for uncorrelated JAM events and events mixed with 90% uncorrelated JAM particles and 10% CMC particles ($\eta = 10\%$). For a smaller replacing rate ($\eta = 5\%$), both validation and training accuracy decrease as compared with ($\eta = 10\%$), whose maximum value is about 81.9%. The validation accuracy is slightly higher than training accuracy caused by the dropout and batch normalization layers used in the network. These two kinds of layers are known to be able to increase the generalization of the network by introducing noise during training.

Shown in Table. I are the testing accuracy of four different configurations. Using the dynamical edge convolution plus point cloud network we constructed in this study, the testing accuracy are 94.7% for 10% replac-

Testing accuracy		
η	Edge-Conv	Point-Cloud Net
5%	82.1%	68.2%
10%	94.7%	79.7%

TABLE I. The testing accuracy for dynamical edge convolution network and a simple point cloud network.

ing rate and 82.1% for 5% replacing rate, which are not quite far away from the validation accuracy. Removing the dynamical edge convolution block, we have tested the performance of the point cloud network with varying numbers of layers and neurons per layer to get the best testing accuracy. The testing accuracy decreases to 79.7% for 10% replacing rate and 68.2% for 5% replacing rate.

B. Interpretability: tagging

To figure out how does the network make its decision in identifying critical fluctuations from the background, we have added a tagging layer to the neural network. To quantify the tagging performance, we introduce two metrics as follows,

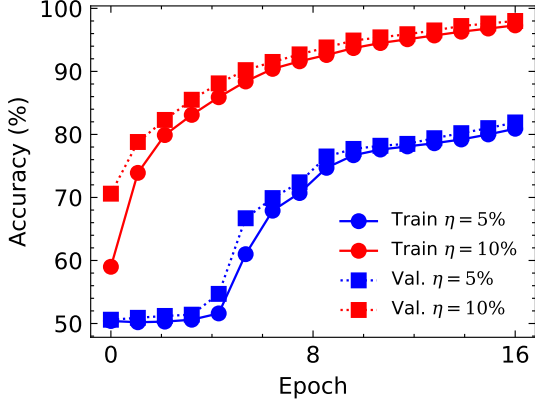


FIG. 3. The training and validation accuracy as a function of epochs. The training accuracy is in solid lines, for replacing rate 10% (above) and 5% (below). The validation accuracy is in dashed lines for replacing rate 10% (above) and 5% (below).

$$r_c = \frac{N_C}{N_C + N_M}, \quad r_t = \frac{N_C}{N_C + N_B} \quad (3)$$

where r_c is the catching rate defined as the ratio between the number of correctly tagged particles N_C and total number of signal particles $N_C + N_M$, where N_M is the number of signal particles missed by the tagging module. r_t is the tagging rate defined as the ratio between the number of correctly tagged particles N_C and the total number of tagged particles $N_C + N_B$, where N_B is the number of wrongly tagged uncorrelated particles.

The average catching rates $r_c = 20.4\%$ for $\eta = 5\%$ and $r_c = 16.7\%$ for $\eta = 10\%$ indicate that the network may use part of the correlated particles to make its decision. On the other hand, the tagging rate $r_t = 73.0\%$ for $\eta = 5\%$ and $r_t = 78.8\%$ for $\eta = 10\%$ are much higher than catching rate r_c . Although the tagging module does not use all signal particles, about 3/4 of the tagged particles are indeed correlated CMC particles carrying critical fluctuations.

Figure 4 demonstrates the output of the tagging module. In the upper subplots, grey dots represent unchanged JAM particles and red dots represent all the critical particles in two testing events. The corresponding tagging output for these two events are shown in the two lower subplots, where the red dots represent critical particles correctly tagged by the network while the blue ones are JAM particles but incorrectly tagged as critical particles. Only part of critical particles are recognized by the tagging module. But as discussed before, the incorrectly tagged particles are much fewer than correctly tagged critical particles. The two figures in the left are for 5% replacing rate while the ones on the right are for 10% replacing rate. In this specific event with 5% replacing rate, only 3 particles are tagged as critical particles, with one of them being incorrect. That explains why the classification performance for 10% replacing rate is much

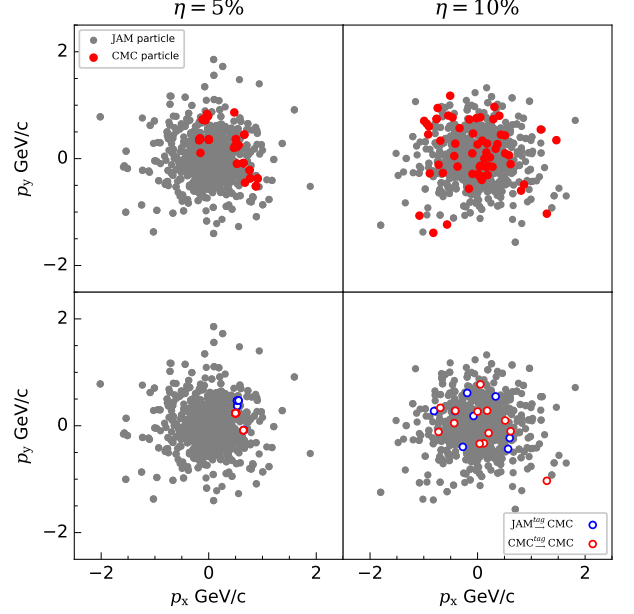


FIG. 4. The upper subplots show the comparison of JAM event and its corresponding CP event, in which the grey dots are the unchanged JAM particles, and the red ones are the critical particles introduced by CMC events. The lower subplots are labeled results of tagging network, and the red dots refer to particles which were tagged correctly, while the blue ones are JAM particles labeled as CMC ones, while the grey dots are unlabeled particles. The graphs on the left show an example of $\eta = 5\%$, while the ones on the right show an example of $\eta = 10\%$.

higher than 5% replacing rate .

IV. SUMMARY AND OUTLOOK

In summary, we have constructed a dynamical edge convolution plus point cloud network to identify the weak intermittency signal from the experimental data of heavy-ion collisions. We have demonstrated that such a state-of-the-art deep learning network enables us to achieve a testing accuracy 82.1% if only 5% of JAM particles in each event are replaced by correlated critical particles. The performance increases to 94.7% if the replacing rate of correlated particles increases to 10%. Removing the dynamical edge convolution block will decrease the performance by a large margin. Using tagging module, we further demonstrate that the network can use part of correlated particles to make their decision. At the same time, only 1/4 of uncorrelated background particles are incorrectly tagged as critical particles.

We observe that the network can identify self-similarity or scaling invariant from uncorrelated background. This is important for experimental data analysis since only one indication of intermittency is observed in Ar + Sc collisions whereas several other systems with similar collision energies fail. Different from previous theoretical

studies, we preserve the single particle distribution while introducing a small fraction of particles with multi particle fractal structure. This is more realistic but also difficult for the traditional intermittency analysis. Based on our study, deep learning shows strong pattern recognition ability in identifying weak intermittency signals associated with critical phenomena. The method developed in this study can be applied to probe the critical fluctuations in heavy-ion collisions and can also be used to explore the criticality of other systems.

ACKNOWLEDGEMENT

We thank Jin Wu for helpful discussions on the critical monte carlo model. This work is supported by the National Key Research and Development Program of China (Grant No. 2020YFE0202002 and 2018YFE0205201), the National Natural Science Foundation of China under Grant Nos. 11935007, 11221504, 11890711, 11861131009 and 12075098, and by the Director, Office of Energy Research, Office of High Energy and Nuclear Physics, Division of Nuclear Physics, of the U.S. Department of Energy (DOE) under grant No. DE-AC02-05CH11231, by the U.S. National Science Foundation under No. OAC-2004571 within the X-SCAPE Collaboration. Computations are performed at Nuclear Science Computer Center at CCNU (NSC3). LG Pang and YG Huang also acknowledge the support provided by Huawei Technologies Co., Ltd.

-
- [1] K. Fukushima and T. Hatsuda, *Rept. Prog. Phys.* **74**, 014001 (2011), [arXiv:1005.4814 \[hep-ph\]](#).
 - [2] A. Bzdak, S. Esumi, V. Koch, J. Liao, M. Stephanov, and N. Xu, *Phys. Rept.* **853**, 1 (2020), [arXiv:1906.00936 \[nucl-th\]](#).
 - [3] X. Luo and N. Xu, *Nucl. Sci. Tech.* **28**, 112 (2017), [arXiv:1701.02105 \[nucl-ex\]](#).
 - [4] Y. Aoki, S. Borsanyi, S. Durr, Z. Fodor, S. D. Katz, S. Krieg, and K. K. Szabo, *JHEP* **06**, 088 (2009), [arXiv:0903.4155 \[hep-lat\]](#).
 - [5] H. T. Ding et al. (HotQCD), *Phys. Rev. Lett.* **123**, 062002 (2019), [arXiv:1903.04801 \[hep-lat\]](#).
 - [6] H.-T. Ding, F. Karsch, and S. Mukherjee, *Int. J. Mod. Phys. E* **24**, 1530007 (2015), [arXiv:1504.05274 \[hep-lat\]](#).
 - [7] C. Shi, Y.-L. Wang, Y. Jiang, Z.-F. Cui, and H.-S. Zong, *JHEP* **07**, 014 (2014), [arXiv:1403.3797 \[hep-ph\]](#).
 - [8] F. Gao and Y.-x. Liu, *Phys. Rev. D* **94**, 076009 (2016), [arXiv:1607.01675 \[hep-ph\]](#).
 - [9] C. S. Fischer, *Prog. Part. Nucl. Phys.* **105**, 1 (2019), [arXiv:1810.12938 \[hep-ph\]](#).
 - [10] W.-J. Fu, J. M. Pawłowski, and F. Rennecke, *Phys. Rev. D* **101**, 054032 (2020), [arXiv:1909.02991 \[hep-ph\]](#).
 - [11] M. A. Stephanov, *Prog. Theor. Phys. Suppl.* **153**, 139 (2004), [arXiv:hep-ph/0402115](#).
 - [12] M. A. Stephanov, *PoS LAT2006*, 024 (2006), [arXiv:hep-lat/0701002](#).
 - [13] J. Hofmann, H. Stoecker, U. W. Heinz, W. Scheid, and W. Greiner, *Phys. Rev. Lett.* **36**, 88 (1976).
 - [14] H. Stoecker and W. Greiner, *Phys. Rept.* **137**, 277 (1986).
 - [15] J. Brachmann, S. Soff, A. Dumitru, H. Stoecker, J. A. Maruhn, W. Greiner, L. V. Bravina, and D. H. Rischke, *Phys. Rev. C* **61**, 024909 (2000), [arXiv:nucl-th/9908010](#).
 - [16] J. Brachmann, A. Dumitru, H. Stoecker, and W. Greiner, *Eur. Phys. J. A* **8**, 549 (2000), [arXiv:nucl-th/9912014](#).
 - [17] L. P. Csernai and D. Rohrlich, *Phys. Lett. B* **458**, 454 (1999), [arXiv:nucl-th/9908034](#).
 - [18] Y. B. Ivanov, E. G. Nikonov, W. Noerenberg, A. A. Shantenko, and V. D. Toneev, *Acta Phys. Hung. A* **15**, 117 (2002), [arXiv:nucl-th/0011004](#).
 - [19] D. H. Rischke, Y. Pursun, J. A. Maruhn, H. Stoecker, and W. Greiner, *Acta Phys. Hung. A* **1**, 309 (1995), [arXiv:nucl-th/9505014](#).
 - [20] H. Stoecker, *Nucl. Phys. A* **750**, 121 (2005), [arXiv:nucl-th/0406018](#).
 - [21] L. P. Csernai, A. Anderlik, C. Anderlik, V. K. Magas, E. Molnar, A. Nyiri, D. Rohrlich, and K. Tamosiunas, *Acta Phys. Hung. A* **22**, 181 (2005), [arXiv:hep-ph/0405277](#).
 - [22] Y. Nara, H. Niemi, J. Steinheimer, and H. Stöcker, *Phys. Lett. B* **769**, 543 (2017), [arXiv:1611.08023 \[nucl-th\]](#).
 - [23] Y. Nara, H. Niemi, A. Ohnishi, J. Steinheimer, X. Luo, and H. Stöcker, *Eur. Phys. J. A* **54**, 18 (2018), [arXiv:1708.05617 \[nucl-th\]](#).
 - [24] Y. Nara, J. Steinheimer, and H. Stoecker, *Eur. Phys. J. A* **54**, 188 (2018), [arXiv:1809.04237 \[nucl-th\]](#).
 - [25] K. Paech, H. Stoecker, and A. Dumitru, *Phys. Rev. C* **68**, 044907 (2003), [arXiv:nucl-th/0302013](#).
 - [26] M. A. Stephanov, *Phys. Rev. Lett.* **102**, 032301 (2009), [arXiv:0809.3450 \[hep-ph\]](#).
 - [27] M. A. Stephanov, *Phys. Rev. Lett.* **107**, 052301 (2011), [arXiv:1104.1627 \[hep-ph\]](#).
 - [28] M. M. Aggarwal et al. (STAR Collaboration), *Phys. Rev. Lett.* **105**, 022302 (2010), [arXiv:1004.4959 \[nucl-ex\]](#).
 - [29] L. Adamczyk et al. (STAR Collaboration), *Phys. Rev. Lett.* **112**, 032302 (2014), [arXiv:1309.5681 \[nucl-ex\]](#).
 - [30] L. Adamczyk et al. (STAR Collaboration), *Phys. Rev. Lett.* **113**, 052302 (2014), [arXiv:1404.1433 \[nucl-ex\]](#).
 - [31] L. Adamczyk et al. (STAR Collaboration), *Phys. Lett. B* **785**, 551 (2018), [arXiv:1709.00773 \[nucl-ex\]](#).
 - [32] J. Adam et al. (STAR), *Phys. Rev. Lett.* **126**, 092301 (2021), [arXiv:2001.02852 \[nucl-ex\]](#).
 - [33] M. Abdallah et al. (STAR), (2021), [arXiv:2101.12413 \[nucl-ex\]](#).
 - [34] M. Nahrgang, S. Leupold, C. Herold, and M. Bleicher, *Phys. Rev. C* **84**, 024912 (2011), [arXiv:1105.0622 \[nucl-th\]](#).
 - [35] C. Herold, M. Nahrgang, I. Mishustin, and M. Bleicher, *Phys. Rev. C* **87**, 014907 (2013), [arXiv:1301.1214 \[nucl-th\]](#).

- [36] C. Plumberg and J. I. Kapusta, *Phys. Rev. C* **95**, 044910 (2017), [arXiv:1702.01368 \[nucl-th\]](#).
- [37] F. Li and C. M. Ko, *Phys. Rev. C* **93**, 035205 (2016), [arXiv:1601.00026 \[nucl-th\]](#).
- [38] O. Scavenius, A. Dumitru, E. S. Fraga, J. T. Lenaghan, and A. D. Jackson, *Phys. Rev. D* **63**, 116003 (2001), [arXiv:hep-ph/0009171](#).
- [39] L. F. Palhares and E. S. Fraga, *Phys. Rev. D* **82**, 125018 (2010), [arXiv:1006.2357 \[hep-ph\]](#).
- [40] C. Herold, M. Nahrgang, I. Mishustin, and M. Bleicher, *Nucl. Phys. A* **925**, 14 (2014), [arXiv:1304.5372 \[nucl-th\]](#).
- [41] F. Li and C. M. Ko, *Phys. Rev. C* **95**, 055203 (2017), [arXiv:1606.05012 \[nucl-th\]](#).
- [42] P. Chomaz, M. Colonna, and J. Randrup, *Phys. Rept.* **389**, 263 (2004).
- [43] J. Randrup, *Phys. Rev. Lett.* **92**, 122301 (2004), [arXiv:hep-ph/0308271](#).
- [44] C. Sasaki, B. Friman, and K. Redlich, *Phys. Rev. Lett.* **99**, 232301 (2007), [arXiv:hep-ph/0702254](#).
- [45] J. Steinheimer and J. Randrup, *Phys. Rev. Lett.* **109**, 212301 (2012), [arXiv:1209.2462 \[nucl-th\]](#).
- [46] J. Steinheimer and J. Randrup, *Phys. Rev. C* **87**, 054903 (2013), [arXiv:1302.2956 \[nucl-th\]](#).
- [47] J. Steinheimer, J. Randrup, and V. Koch, *Phys. Rev. C* **89**, 034901 (2014), [arXiv:1311.0999 \[nucl-th\]](#).
- [48] K.-J. Sun, L.-W. Chen, C. M. Ko, J. Pu, and Z. Xu, *Phys. Lett. B* **781**, 499 (2018), [arXiv:1801.09382 \[nucl-th\]](#).
- [49] N. Yu, D. Zhang, and X. Luo, *Chin. Phys. C* **44**, 014002 (2020), [arXiv:1812.04291 \[nucl-th\]](#).
- [50] K.-J. Sun, C. M. Ko, F. Li, J. Xu, and L.-W. Chen, (2020), [arXiv:2006.08929 \[nucl-th\]](#).
- [51] W. Zhao, K.-j. Sun, C. M. Ko, and X. Luo, (2021), [arXiv:2105.14204 \[nucl-th\]](#).
- [52] K. Wilson and J. B. Kogut, *Phys. Rept.* **12**, 75 (1974).
- [53] T. D. Lee and C. N. Yang, *Phys. Rev.* **87**, 410 (1952).
- [54] M. S. Pradeep and M. Stephanov, *Phys. Rev. D* **100**, 056003 (2019), [arXiv:1905.13247 \[hep-ph\]](#).
- [55] J. M. Stafford, D. Mroczek, A. R. Nava Acuna, J. Noronha-Hostler, P. Parotto, D. R. P. Price, and C. Ratti, (2021), [arXiv:2103.08146 \[hep-ph\]](#).
- [56] D. Teaney, *Nucl. Phys. A* **1005**, 121750 (2021).
- [57] M. Bluhm et al., *Nucl. Phys. A* **1003**, 122016 (2020), [arXiv:2001.08831 \[nucl-th\]](#).
- [58] A. Bialas and R. B. Peschanski, *Nucl. Phys. B* **308**, 857 (1988).
- [59] H. Satz, *Nucl. Phys. B* **326**, 613 (1989).
- [60] R. C. Hwa, *Phys. Rev. D* **41**, 1456 (1990).
- [61] N. Antoniou, Y. Contoyannis, F. Diakonou, A. Karanikas, and C. Ktorides, *Nucl. Phys. A* **693**, 799 (2001), [arXiv:hep-ph/0012164](#).
- [62] J. Wu, Y. Lin, Y. Wu, and Z. Li, *Phys. Lett. B* **801**, 135186 (2020), [arXiv:1901.11193 \[nucl-th\]](#).
- [63] T. Anticic et al. (NA49), *Eur. Phys. J. C* **75**, 587 (2015), [arXiv:1208.5292 \[nucl-ex\]](#).
- [64] N. Davis (NA61/SHINE), *PoS EPS-HEP2019*, 305 (2020).
- [65] N. Davis, N. Antoniou, and F. K. Diakonou (NA61/Shine), *PoS CORFU2018*, 154 (2019).
- [66] L.-G. Pang, K. Zhou, N. Su, H. Petersen, H. Stöcker, and X.-N. Wang, *Nature Commun.* **9**, 210 (2018), [arXiv:1612.04262 \[hep-ph\]](#).
- [67] L.-G. Pang, *Nucl. Phys. A* **1005**, 121972 (2021).
- [68] Y.-L. Du, K. Zhou, J. Steinheimer, L.-G. Pang, A. Motornenko, H.-S. Zong, X.-N. Wang, and H. Stöcker, *Eur. Phys. J. C* **80**, 516 (2020), [arXiv:1910.11530 \[hep-ph\]](#).
- [69] Y. Kvasiuk, E. Zabrodin, L. Bravina, I. Didur, and M. Frolov, *JHEP* **07**, 133 (2020), [arXiv:2004.14409 \[nucl-th\]](#).
- [70] J. Steinheimer, L. Pang, K. Zhou, V. Koch, J. Randrup, and H. Stoecker, *JHEP* **12**, 122 (2019), [arXiv:1906.06562 \[nucl-th\]](#).
- [71] M. O. Kuttan, K. Zhou, J. Steinheimer, A. Redelbach, and H. Stoecker, (2021), [arXiv:2107.05590 \[hep-ph\]](#).
- [72] R. Wang, Y.-G. Ma, R. Wada, L.-W. Chen, W.-B. He, H.-L. Liu, and K.-J. Sun, *Phys. Rev. Res.* **2**, 043202 (2020), [arXiv:2010.15043 \[nucl-th\]](#).
- [73] Y. Nara, N. Otuka, A. Ohnishi, K. Niita, and S. Chiba, *Phys. Rev. C* **61**, 024901 (2000), [arXiv:nucl-th/9904059](#).
- [74] Nara, Yasushi, *EPJ Web Conf.* **208**, 11004 (2019).
- [75] H. Sorge, *Phys. Rev. C* **52**, 3291 (1995).
- [76] H. Sorge, *Physics Letters B* **402**, 251 (1997).
- [77] S. Bass, M. Belkacem, M. Bleicher, M. Brandstetter, L. Bravina, C. Ernst, L. Gerland, M. Hofmann, S. Hofmann, J. Konopka, G. Mao, L. Neise, S. Soff, C. Spieles, H. Weber, L. Winkelmann, H. Stöcker, W. Greiner, C. Hartnack, J. Aichelin, and N. Amelin, *Progress in Particle and Nuclear Physics* **41**, 255 (1998).
- [78] M. Bleicher, E. Zabrodin, C. Spieles, S. A. Bass, C. Ernst, S. Soff, L. Bravina, M. Belkacem, H. Weber, H. Stöcker, and W. Greiner, *Journal of Physics G: Nuclear and Particle Physics* **25**, 1859 (1999).
- [79] S. H. Kahana, D. E. Kahana, Y. Pang, and T. J. Schlagel, *Annual Review of Nuclear and Particle Science* **46**, 31 (1996), <https://doi.org/10.1146/annurev.nucl.46.1.31>.
- [80] B.-A. Li and C. Ko, *Nuclear Physics A* **630**, 556 (1998), nucleus-Nucleus Collisions.
- [81] Z.-W. Lin, C. M. Ko, B.-A. Li, B. Zhang, and S. Pal, *Phys. Rev. C* **72**, 064901 (2005).
- [82] J. Weil et al., *Phys. Rev. C* **94**, 054905 (2016), [arXiv:1606.06642 \[nucl-th\]](#).
- [83] N. G. Antoniou, F. K. Diakonou, A. S. Kapoyannis, and K. S. Kousouris, *Phys. Rev. Lett.* **97**, 032002 (2006), [arXiv:hep-ph/0602051](#).